The Dynamics of Lead-Screw Drives: Low-Order Modeling and Experiments

Kripa K. Varanasi

Samir A. Nayfeh

Department of Mechanical Engineering
Massachusetts Institute of Technology
Cambridge, Massachusetts

The closed-loop performance of a lead-screw drive is usually limited by a resonance in which the carriage oscillates in the direction of motion as the screw undergoes longitudinal and torsional deformation. In this paper, we develop a model of lead-screw system dynamics that accounts for the distributed inertia of the screw and the compliance and damping of the thrust bearings, nut, and coupling. The distributed-parameter model of the lead-screw drive system is reduced to a low-order model using a Galerkin procedure and verified by experiments performed on a pair of ball-screw systems. The model is found to accurately predict the presence of a finite right-half plane zero in the transfer function from motor torque to carriage position. A viscoelastic damper incorporated into one of the lead-screw support bearings is shown to give rise to significant, deterministic damping in the system transfer functions. [DOI: 10.1115/1.1771690]

1 Introduction

Lead-screw drives are often used in high-performance linear-motion systems because they provide a transmission with a relatively high stiffness and an inherent drive reduction. Low-friction ball or roller screws provide acceptably smooth motion for many applications because of elastic averaging among many balls or rollers in simultaneous contact, and they are readily preloaded to have no backlash. One disadvantage of a lead-screw is that the rotary inertia of the screw makes it difficult to achieve high accelerations using a motor of a given size. A second, and still poorly understood, limitation on the dynamic performance of a lead-screw drive arises from a resonance in which the carriage oscillates in the direction of motion as the screw undergoes longitudinal and torsional deformation.

If feedback is taken from a sensor attached to the motor, the rotation of the motor can usually be controlled very rapidly and precisely. But the carriage position is unknown, and it can deviate from that desired due to quasi-static effects (such as form errors or thermal expansion) as well as resonant response of the drive. Moreover, no matter how high the bandwidth of motor control, the carriage response rolls off rapidly after the first drive resonance. If instead feedback is taken from the carriage position, the quasi-static errors can be eliminated, but the controller bandwidth is limited in practice to be significantly smaller than the frequency of the first drive resonance. In this paper, we develop a model of the dynamics of a lead-screw drive system that correctly accounts for the distributed inertia of the screw but is simple enough to use for simultaneous design of the mechanical system and controller.

1.1 Background

Several researchers have studied the effect of control strategies on the performance of lead-screw systems. Chen and Tlusty [1] study the effects of feedback from motor and carriage position. Tlusty [2] provides a discussion of various control strategies for positional servomechanisms and suggests various measures such as feed-forward compensation and accelerometric feedback for improving the performance of lead-screw drives. Smith [3] considers lead-screws systems with motor-position feedback and employs a finite-element model to study the higher-order (predominantly torsional) modes of vibration. Smith et al. [4] implement adaptive control techniques to enhance the performance of a machine tool axis. Lim et al. [5] implement a torsional displacement feedback algorithm and an estimation method for torsional displacement to reduce the error in the position of an *XY* table driven by motors via ball-screws.

In this paper, we develop a model for the first resonance of a lead-screw drive of the configuration sketched in Fig. 1. It consists of a screw constrained to the machine base by means of rotary bearings and driven by a motor via a flexible coupling. The nut is mounted to the carriage which is constrained to move axially on linear bearings. The end of the screw nearest the drive motor is axially constrained to the base by means of a thrust bearing.

During operation of the mechanism, friction between the screw and the nut generates significant heat, leading to a temperature rise and thermal expansion in the screw. To accommodate this expansion, the screw is often allowed to slide freely in the axial direction at the support bearing farthest from the motor. Thus, the entire thrust load is transmitted to the base through the serial combination of the elements between the motor-side thrust bearings and the carriage. Because the compliance of the screw increases with increasing length, the frequency of the resonance in such a system decreases to its lowest value when the carriage is at the end farthest from the motor.

In heavy machine tools it is sometimes practical to constrain the screw by thrust bearings at both ends and pre-stretch the screw during assembly by large enough a displacement that some tension is maintained even when the screw becomes hot. Such systems exhibit relatively high resonant frequencies and small thermal errors. But the required preload is often so high that it requires relatively large thrust bearings and results in significant warping of the machine base. Nayfeh [6] and Nayfeh and Slocum [7] propose that a viscoelastic element be inserted into the load path at the thrust bearing farthest from the motor. Such a viscoelastic damper can be made compliant enough that the required pre-loading displacement is attained with relatively small loads while still giving rise to significant damping in the system.

1.2 Approach. Damping plays a key role in determining the effects of resonance on closed-loop performance [8]. Most of the damping in machines arises at material interfaces and is difficult to model from first principles [9–11]. This damping is often modeled as ''structural'' or ''hysteretic'' and introduced into a frequency-domain model by assigning complex-valued stiffnesses to lossy elements of a system (e.g., Nashif et al. [12]). In this

Contributed by the Dynamic Systems, Measurement, and Control Division of THE AMERICAN SOCIETY OF MECHANICAL ENGINEERS for publication in the ASME JOURNAL OF DYNAMIC SYSTEMS, MEASUREMENT, AND CONTROL. Manuscript received by the ASME Dynamic Systems and Control Division January 3, 2003; final revision, September 22, 2003. Associate Editor: C. D. Rahn.

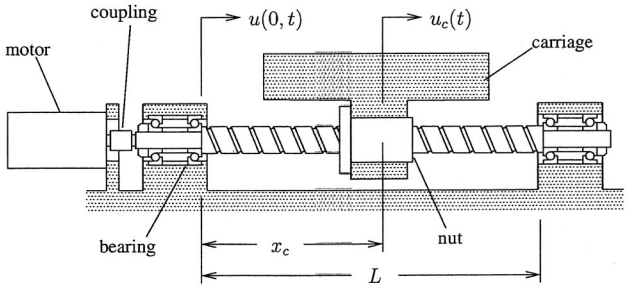

Fig. 1 Sketch of a ball-screw drive

paper, we develop a model of the system in the frequency domain so that hysteretic damping can be incorporated by use of a complex stiffness to describe the bearings or nut. We then obtain an equivalent viscously damped model suitable for prediction of the transient response and design of controllers.

We begin by writing second-order wave equations in the frequency domain for the longitudinal and torsional dynamics of the screw along with boundary conditions that take into account the compliance (and possible damping) of the bearings and the nut. We argue that unless the effective inertia of the screw is much larger than that of the carriage and motor, the mode shape associated with the first resonance will be close to the shape obtained from quasi-static deformation of the system. A Galerkin procedure based on this mode shape yields a consistent mass matrix in a reduced-order model with the rotation of the motor and position of the carriage as coordinates. Next, for light damping, we use a perturbation expansion to determine approximations to the open-loop poles of the system and thence derive an equivalent set of time-domain equations.

Finally, we verify the model against measurements performed on a pair of ball-screw drives. Modal tests yield experimentally the mode shape associated with the axial drive resonance. Measurements of transfer functions from motor torque to both motor rotation and carriage position provide a direct comparison with the model. We find generally good agreement between the experiment and model (with and without a viscoelastic damper), confirming that the model is suitable for prediction of the response of the system over the frequency range of interest. As predicted by the model, we find that a non-minimum phase zero in the transfer function from motor torque to carriage position arises from the distributed inertia of the screw.

2 Modeling

Consider steady harmonic vibration of the lead-screw drive shown in Fig. 1 at a frequency ω, where the vibratory displacement of the carriage is given by $\mathrm{Re}(u_c(\omega)e^{j\omega t})$ and the angle of rotation of the motor is given by $\mathrm{Re}(\theta_m(\omega)e^{j\omega t})$. The complex variables $u_c(\omega)$ and $\theta_m(\omega)$ each represent the magnitude and phase of the motion as a function of the frequency ω. The displacement and angle of twist of the screw vary along the length of the screw and hence are written as $\mathrm{Re}(u(x,\omega)e^{j\omega t})$ and $\mathrm{Re}(\theta(x,\omega)e^{j\omega t})$.

2.1 Distributed-Parameter Model. The longitudinal displacement $u(x,\omega)$ and angle of rotation $\theta(x,\omega)$ of the screw are each governed by a second-order wave equation. Neglecting the effect of the threads on the cross-sectional properties of the screw, we write

$$Eu''(x,\omega)+\rho\omega^2 u(x,\omega)=0 \quad \text{and} \quad G\theta''(x,\omega)+\rho\omega^2\theta(x,\omega)=0 \tag{1}$$

where the primes denote partial differentiation with respect to x, ρ is the density of the screw, and E and G are, respectively, its extensional and shear moduli.

2.1.1 End Conditions. At the end of the screw nearest the motor (at $x=0$), the longitudinal force must match the longitudinal force in the thrust bearing. If k_{b1} represents the combined longitudinal stiffness of the thrust bearing and its housing, this condition takes the form

$$EAu'(0,\omega)=k_{b1}u(0,\omega) \tag{2}$$

where A is the average cross-sectional area of the screw and the prime denotes partial differentiation with respect to x. Similarly, denoting the effective stiffness at the end farthest from the motor as k_{b2}, we have

$$EAu'(L,\omega)=k_{b2}u(L,\omega) \tag{3}$$

The value of k_{b2} can be set to zero if the screw is axially unrestrained at this end.

At $x=L$, the twisting moment on the screw must vanish. This condition takes the form $\theta'(L,\omega)=0$. At $x=0$, the twisting moment in the screw must match that in the coupling. Denoting the torsional stiffness of the coupling between the motor and screw as κ_c, we relate the rotation at the end of the screw to the rotation $\theta_m(\omega)$ of the motor by

$$GJ\theta'(0,\omega)=\kappa_c[\theta(0,\omega)-\theta_m(\omega)] \tag{4}$$

where J is the (average) second polar moment of the cross-section of the screw.

2.1.2 Conditions at the Nut. If the carriage (more precisely, the nut) is located at a position $x=x_c$ along the length of the screw and the interface between the nut and the screw is perfectly rigid, the carriage displacement u_c would be obtained from the screw's longitudinal displacement plus its angle of twist times the drive ratio:

$$u_c(\omega)=u(x_c,\omega)+\theta(x_c,\omega)\frac{\ell}{2\pi} \tag{5}$$

where ℓ is the lead of the screw (i.e., the distance by which the thread advances in one rotation). But often, the interface between the screw and the nut as well as the means by which the nut is mounted to the carriage have appreciable compliance. We define the axial stiffness k_n of the nut as the ratio of the axial force F_n developed in the screw and the resulting displacement $u_c(\omega)$ of the carriage if the screw is restrained from displacement or rotation at x_c.

The axial force and the torque developed in the screw are given by the combination of the forces and torques on the portions of the screw to the left and to the right of the nut according to

$$F_n=EA[u'(x_c^+,\omega)-u'(x_c^-,\omega)] \tag{6}$$

Making use of this expression, we rewrite the kinematic relationship (5) as

$$u_c(\omega)=u(x_c,\omega)+\frac{EA}{k_n}[u'(x_c^-,\omega)-u'(x_c^+,\omega)]+\frac{\ell}{2\pi}\theta(x_c,\omega) \tag{7}$$

which is the desired equation relating the displacement of the carriage to the displacement and rotation of the screw at x_c.

2.1.3 Motor and Carriage. The motor armature is subject to the twisting moment $\kappa_c[\theta(0,\omega)-\theta_m(\omega)]$ imposed by the screw on the coupling in addition to the actuation torque $T_m(\omega)$ and an effective viscous damping torque $j\omega C_m\theta_m(\omega)$. The equation of motion of the motor armature therefore takes the form

$$(-\omega^2 J_m+j\omega C_m+\kappa_c)\theta_m(\omega)=T_m+\kappa_c\theta(0,\omega) \tag{8}$$

where J_m is the rotary inertia of the motor armature.

The carriage is subject to the force exerted by the screw on the nut in addition to a disturbance force $F_c(\omega)$ and an effective viscous damping force $j\omega C_c u_c(\omega)$. We therefore write

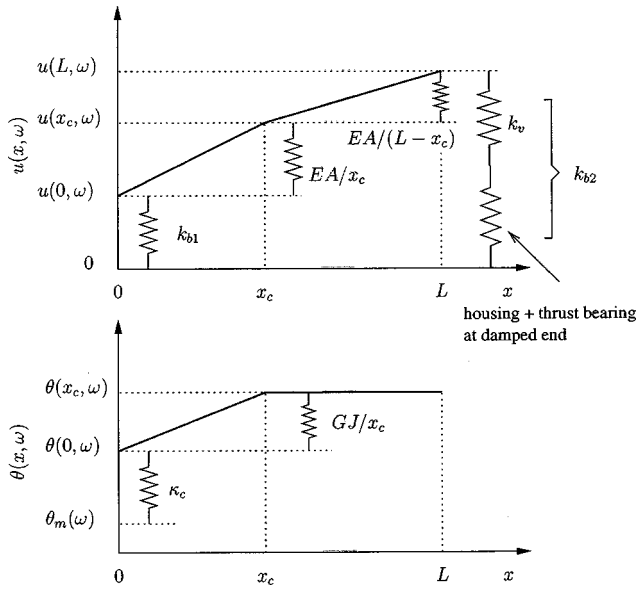

Fig. 2 Quasi-static displacement

$$(-\omega^2 m_c + j\omega C_c + k_n)u_c(\omega) = F_c(\omega) + k_n\left[u(x_c,\omega) + \theta(x_c,\omega)\frac{\ell}{2\pi}\right] \tag{9}$$

where m_c is the mass of the carriage.

2.2 Lumped-Parameter Approximation. Longitudinal waves in the screw travel at a speed of $(E/\rho)^{1/2}$. If the frequency of motion ω is much lower than the time that it takes for such a wave to travel the length of the screw (that is, if $\omega L \ll (E/\rho)^{1/2}$), the inertia terms in (1) are small and longitudinal wave propagation in the screw can be neglected. Under this condition, the displacement $u(x,\omega)$ of the screw varies approximately linearly with x on each portion of the screw between the nut and the thrust bearings (as sketched in Fig. 2) over the frequency range of interest. Likewise, if the shear modulus of the screw is G, torsional waves travel at a speed of $(G/\rho)^{1/2}$ and torsional waves can be neglected if $\omega L \ll (G/\rho)^{1/2}$. Under this condition, $\theta(x,\omega)$ varies approximately linearly with x on the portion of the screw between the nut and the motor and is constant on the remainder of the screw.

In Section 2.2.1, we neglect the inertia of the system and examine the deformation obtained if the carriage is subjected to a longitudinal displacement $u_c(\omega)$ and the motor is subjected to a rotation $\theta_m(\omega)$. That is, we consider what happens at very small ω, where the longitudinal and torsional deformation of the screw appear as shown in Fig. 2. Then, in Section 2.2.2, we perform a Galerkin approximation based on the quasi-static deformation to obtain a low-order model with the motor rotation and carriage displacement as coordinates.

2.2.1 Quasi-Static Displacements. Let us now impose a quasi-static (slowly varying) carriage displacement $u_c(\omega)$ and motor rotation $\theta_m(\omega)$ by means of a longitudinal force F exerted on the carriage and a torque $-F\ell/2\pi$ exerted on the motor. The forces and displacements are related by

$$F = k_t\left[u_c(\omega) - \theta_m(\omega)\frac{\ell}{2\pi}\right] \tag{10}$$

where k_t is the total stiffness of the system (which we obtain later) and we have neglected the inertia effects. We wish to solve for the quasi-static displacement of the system, which takes the form given in Fig. 2, so we need only solve for $u(x,\omega)$ and $\theta(x,\omega)$ at the location of the nut and at the ends of the screw.

Making use of Eq. (4) and the piecewise-linear dependence of θ on x, we write the angular displacements at $x=0$ and x_c in terms of $u_c(\omega)$ and $\theta_m(\omega)$ as

$$\begin{pmatrix} \theta(0,\omega) - \theta_m(\omega) \\ \theta(x_c,\omega) - \theta_m(\omega) \end{pmatrix} = \begin{pmatrix} 1/\kappa_c \\ 1/\kappa_{tc} \end{pmatrix} \frac{k_t \ell}{2\pi}\left[u_c(\omega) - \theta_m(\omega)\frac{\ell}{2\pi}\right] \tag{11}$$

where

$$\kappa_{tc} = \frac{1}{\kappa_c} + \frac{x_c}{GJ} \tag{12}$$

That is, the angle of twist of the screw relative to the motor is governed by the serial compliances $1/\kappa_c$ and x_c/GJ of the coupling and screw, respectively.

To obtain similar expressions for the longitudinal displacement at $x=0$, x_c, and L, we find it convenient to introduce terms for the stiffness of the screw and thrust bearings to the left and to the right of the nut. Making use of (2) and (3), we write them, respectively, as

$$k_1 = \left(\frac{x_c}{EA} + \frac{1}{k_{b1}}\right)^{-1} \quad \text{and} \quad k_2 = \left(\frac{L-x_c}{EA} + \frac{1}{k_{b2}}\right)^{-1} \tag{13}$$

Noting that the total force F given by Eq. (10) is divided among the portions of the screw to the left and right of the nut, we write the longitudinal displacements as

$$\begin{pmatrix} u(0,\omega) \\ u(x_c,\omega) \\ u(L,\omega) \end{pmatrix} = \begin{pmatrix} k_2/k_{b1} \\ 1 \\ k_1/k_{b2} \end{pmatrix} \frac{k_t}{k_1+k_2}\left[u_c(\omega) - \theta_m(\omega)\frac{\ell}{2\pi}\right] \tag{14}$$

Finally, we combine the second row of Eq. (11), the middle row of Eq. (14), and Eq. (10) to obtain an expression for the total stiffness k_t:

$$k_t = \left[\frac{1}{k_1+k_2} + \frac{1}{k_n} + \left(\frac{\ell}{2\pi}\right)^2\left(\frac{1}{\kappa_c} + \frac{x_c}{GJ}\right)\right]^{-1} \tag{15}$$

The term k_1+k_2 represents the total axial stiffness of the screw and thrust bearings, which acts in series with (i.e., is subject to the same force as) the nut of stiffness k_n. The first two terms in this expression therefore represent the total longitudinal stiffness of the screw, which acts in series with the total torsional stiffness of the screw multiplied by the square of the drive ratio $\ell/2\pi$.

2.2.2 Dynamic Equations. Based on the discussion given in Section 2.2, the solution of the wave equations given by Eq. (1) coupled with Eqs. (8) and (9) can be approximated by the quasi-static shape shown in Fig. 2 provided that the frequency of motion ω is well below $(E/\rho L^2)^{1/2}$ and $(G/\rho L^2)^{1/2}$. We perform this approximation by minimizing the error in a Galerkin-type (e.g., [9]) weighted residual R of the form

$$\begin{aligned} R = {} & \theta_m(\omega)[(-\omega^2 J_m + j\omega C_m + \kappa_c)\theta_m(\omega) - T_m - \kappa_c\theta(0,\omega)] \\ & + u_c(\omega)\left[(-\omega^2 m_c + j\omega C_c + k_n)u_c(\omega) - F_c - k_n\left(u(x_c,\omega) + \theta(x_c,\omega)\frac{\ell}{2\pi}\right)\right] - \int_0^L u(x,\omega)[Eu''(x,\omega) + \rho\omega^2 u(x,\omega)]dx \\ & - \int_0^L \theta(x,\omega)[G\theta''(x,\omega) + \rho\omega^2\theta(x,\omega)]dx \end{aligned} \tag{16}$$

If the motor rotation $\theta_m(\omega)$ is an approximate solution to Eq. (8) governing the dynamics of the motor, the first line of this expression represents the error in satisfying Eq. (8) weighted by $\theta_m(\omega)$.

The second, third, and fourth lines are similarly formed weighted residuals for the carriage, longitudinal motion of the screw, and torsional motion of the screw.

Because the measurable inputs and outputs of the system are at the motor and carriage, their displacements $u_c(\omega)$ and $\theta_m(\omega)$ are convenient generalized coordinates for the model. We therefore substitute the quasi-static solution in terms of $u_c(\omega)$ and $\theta_m(\omega)$ given by Eqs. (11), (14), and Fig. 2 into the residual given by Eq. (16) and set $\partial R/\partial u_c$ and $\partial R/\partial \theta_m$ to zero, which yields a set of equations that minimize the residual of the dynamic equations over all possible quasi-static deformations. These equations can be written in the familiar second-order form

$$(-\omega^2\mathbf{M}+j\omega\mathbf{C}+\mathbf{K})\begin{pmatrix} u_m(\omega) \\ u_c(\omega)\end{pmatrix}=\begin{pmatrix} F_m \\ F_c\end{pmatrix} \tag{17}$$

where we have introduced an equivalent motor displacement $u_m=(\ell/2\pi)\theta_m$ and an equivalent motor force $F_m=(2\pi/\ell)T_m$.

2.2.3 Mass Matrix. Introducing the notation $n=2\pi/\ell$ for the system drive ratio, we write the mass matrix $\mathbf{M}$ in the form

$$\mathbf{M}=\begin{bmatrix} m_{11} & m_{12} \\ m_{12} & m_{22}\end{bmatrix}=\begin{bmatrix} n^2(J_m+J_1)+m & n^2J_{12}-m \\ n^2J_{12}-m & n^2J_2+m+m_c\end{bmatrix} \tag{18}$$

The term m, which appears in each of the four elements of the mass matrix, is the effective longitudinal inertia of the screw. It is given by

$$m=\rho A\left(\frac{k_t}{k_1+k_2}\right)^2\left[\frac{x_c}{3}\left(1+\frac{k_1}{k_{b1}}+\frac{k_1^2}{k_{b1}^2}\right)+\frac{L-x_c}{3}\left(1+\frac{k_2}{k_{b2}}+\frac{k_2^2}{k_{b2}^2}\right)\right] \tag{19}$$

where A is the average cross-sectional area of the screw. If the motor is locked, the factor $k_t/(k_1+k_2)$ is the ratio of the longitudinal displacement of the screw at x_c to that of the carriage and the terms within the brackets give the contributions to the inertia from the segments of the screw to the left and to the right of the carriage. Often, the thrust bearing at the motor end can be made much stiffer than the screw, so that $k_{b1}\gg k_1$ and the coefficient of x_c approaches 1/3. In contrast, if the bearing farthest from the motor is allowed to slide axially, $k_{b2}=0$ and $k_2/k_{b2}=1$ so that the associated coefficient becomes unity, meaning that all of the mass of the portion of the screw to the right of the carriage becomes associated with the motion of the screw at x_c.

The upper left element of the mass matrix includes the inertia n^2J_m of the motor as well as a contribution from the rotary inertia of the screw given by n^2J_1 where

$$\frac{J_1}{\rho JL}=\left(1-\frac{k_t}{n^2\kappa_{tc}}\right)^2\left\{\frac{x_c}{3L}\left[1+\left(1-\frac{k_t}{n^2\kappa_c}\right)\left(1-\frac{k_t}{n^2\kappa_{tc}}\right)^{-1}+\left(1-\frac{k_t}{n^2\kappa_c}\right)^2\left(1-\frac{k_t}{n^2\kappa_{tc}}\right)^{-2}\right]+\left(1-\frac{x_c}{L}\right)\right\} \tag{20}$$

and J is the average second polar moment of the screw. If the carriage position is locked, the factor $(1-k_t/n^2\kappa_{tc})$ is the ratio of the angular position of the screw θ at $x=x_c$ to the angular position θ_m of the motor; likewise, $(1-k_t/n^2\kappa_c)$ is the ratio of θ at $x=0$ to θ_m.

The lower right element of the mass matrix includes the inertia m_c of the carriage as well as a contribution from the rotary inertia of the screw given by n^2J_2 where

$$\frac{J_2}{\rho JL}=\left(\frac{k_t}{n^2\kappa_{tc}}\right)^2\left[\frac{x_c}{3L}\left(1+\frac{\kappa_{tc}}{\kappa_c}+\frac{\kappa_{tc}^2}{\kappa_c^2}\right)+\left(1-\frac{x_c}{L}\right)\right] \tag{21}$$

The off-diagonal terms include components of the rotary inertia of the screw given by n^2J_{12} where

$$\frac{J_{12}}{\rho JL}=\frac{k_t}{n^2\kappa_{tc}}\left\{\frac{x_c}{L}\left[\frac{1}{6}+\frac{\kappa_{tc}}{\kappa_c}\left(\frac{1}{2}-\frac{k_t}{3n^2\kappa_c}\right)-\frac{k_t}{6n^2\kappa_c}\right]+\left(1-\frac{2x_c}{3L}\right)\left(1-\frac{k_t}{n^2\kappa_{tc}}\right)\right\} \tag{22}$$

These expressions simplify considerably if the coupling and nut are made to have very large torsional stiffnesses.

2.2.4 Stiffness and Damping Matrices. The Galerkin procedure yields relatively simple damping and stiffness matrices:

$$\mathbf{C}=\begin{bmatrix} n^2C_m & 0 \\ 0 & C_c\end{bmatrix} \text{ and } \mathbf{K}=k_t\begin{bmatrix} 1 & -1 \\ -1 & 1\end{bmatrix} \tag{23}$$

But most of the damping in the machine will arise from material interfaces, and is difficult to model from first principles [10,11]. Many experiments show that the energy dissipated at material interfaces—or by viscoelastic materials—depends only moderately on the frequency of vibration; hence it is often incorporated into a model as ''hysteretic'' or ''structural'' damping by augmentation of the stiffness with an imaginary part (e.g., Nashif et al. [12,13]). Such a model makes sense only in the frequency domain, but is useful for prediction of the damping associated with resonances occurring in a given frequency range.

To incorporate hysteretic damping into the model, we replace the real-valued stiffness k_t by a complex stiffness $\hat{k}_t(1+j\eta\,\mathrm{sgn}\,\omega)$ where η is the loss factor associated with the total stiffness k_t. It can be computed by augmenting with a complex part any of the component stiffnesses in the expression for k_t given by Eq. (15).

2.2.5 Approximate Open-Loop Poles. If the system is lightly damped, approximate expressions for the open-loop poles (eigenvalues) of this fourth-order system with complex stiffness can be obtained from a perturbation expansion. That is, if $\omega C_c/k_t$, $\omega n^2C_m/k_t$ and η are of order ϵ, we seek approximations to the poles in the from 0, $-\sigma$, and $-\sigma_d\pm j\omega_d$, where σ and σ_d are of order ϵ. Substituting these expressions into the characteristic equation and equating terms of like orders of ϵ, we obtain

$$\sigma=\frac{n^2C_m+C_c}{n^2(J_m+\rho JL)+m_c} \tag{24}$$

This real-valued pole is associated with motion of the system without deformation of the screw. Hence its value is given by the ratio of the damping and inertia associated with this ''rigid-body'' motion. The longitudinal resonance of the ball-screw system is characterized by the poles $-\sigma_d\pm j\omega_d$ where

$$\omega_d^2=\hat{k}_t\frac{n^2(J_m+\rho JL)+m_c}{m_{11}m_{22}-m_{12}^2} \tag{25}$$

and

$$\sigma_d=\frac{1}{2}\left[\frac{n^2C_m(m_{22}+m_{12})^2+C_c(m_{11}+m_{12})^2}{[n^2(J_m+\rho JL)+m_c]^2(m_{11}m_{22}-m_{12}^2)}+\eta\omega_d\right] \tag{26}$$

where m_{11}, m_{22}, and m_{12} are the elements of the mass matrix as indicated in Eq. (18).

2.2.6 Equivalent Viscous Model. All modeling in this paper thus far has been done in the frequency domain in order to incorporate hysteretic damping in a consistent manner. But the transient response of a system is most easily obtained from a time-domain model. Having obtained (approximate) expressions for the open-loop poles of the system, we can write a model with only viscous damping that has the same approximate poles as the system with hysteretic damping:

$$\mathbf{M}\begin{pmatrix}\ddot{u}_m(t)\\ \ddot{u}_c(t)\end{pmatrix}+\mathbf{C}_e\begin{pmatrix}\dot{u}_m(t)\\ \dot{u}_c(t)\end{pmatrix}+\mathbf{K}_e\begin{pmatrix}u_m(t)\\ u_c(t)\end{pmatrix}=\begin{pmatrix}f_m(t)\\ f_c(t)\end{pmatrix} \tag{27}$$

where

$$\mathbf{C}_e=\mathbf{C}+\frac{\eta\hat{k}_t}{\omega_d}\begin{pmatrix}1 & -1\\ -1 & 1\end{pmatrix} \text{ and } \mathbf{K}_e=\hat{k}_t\begin{pmatrix}1 & -1\\ -1 & 1\end{pmatrix} \quad (28)$$

The matrices **M** and **C** are given by Eqs. (18) and (23) and ω_d is as defined in Eq. (25). A perturbation expansion for light damping (like that described in the previous section) yields the same approximate open-loop poles as given by Eqs. (24)–(26).

Using Eqs. (18)–(22) and (27), we write the collocated transfer function (from the equivalent motor torque to motor rotation) as

$$G_{p1}(s)=\frac{U_m(s)}{F_m(s)}=\frac{m_{22}s^2+(C_c+\eta k_t/\omega_d)s+\hat{k}_t}{\Delta(s)} \quad (29)$$

where $\Delta(s)=\det[\mathbf{M}s^2+\mathbf{C}_e s+\mathbf{K}_e]$ is the characteristic polynomial of the equivalent system. The pair of complex zeros in this transfer function correspond to vibration of the carriage when the motor is locked. The non-collocated transfer function (from equivalent motor torque to carriage position) is given by

$$G_{p2}(s)=\frac{U_c(s)}{F_m(s)}=\frac{-m_{12}s^2+(\eta k_t/\omega_d)s+\hat{k}_t}{\Delta(s)} \quad (30)$$

The non-minimum phase (i.e., right-half plane) zero that appears in this transfer function places a limitation on the closed-loop performance that can be achieved (e.g., [14,15]).

3 Experiments

In this section, we detail measurements made on two ball-screw drives. The ''small stage'' shown in Fig. 3 moves a carriage of mass 25 kg through a travel of 360 mm, whereas the ''large stage'' shown in Fig. 7 moves a carriage whose mass is 80 kg through a travel of 915 mm. For each of the two stages, we measure the transfer functions from motor torque to carriage position and compare the results with those predicted by the model. For the large stage, we also compare the dynamics with and without a damper inserted at the end of the screw farthest from the motor. In addition, we perform a set of modal tests on the large stage to determine the mode shape associated with the measured resonance.

3.1 Small Stage. The ball-screw stage shown in Fig. 3 has a travel of approximately 360 mm. The important details of its construction are given in Table 1 and the details of its design and construction are given by Hochmuth [16]. The motor (Aerotech model BM200 [17]) is attached to the screw by means of a disk-type coupling [18] as shown in Fig. 4. The screw is constrained by a pair of 45-deg-angular contact bearings at the end nearest the motor and allowed to slide axially at the end farthest from the motor. The expected stiffness from this bearing pair is 140 N/μm, but the pillow block that holds these two bearings is attached to the base using only two machine screws over a narrow contact area (see Fig. 4). Using a dial indicator to measure the displacement of the end of the screw under a known applied force, we find that the total stiffness k_{b1} is in fact 51 N/μm.

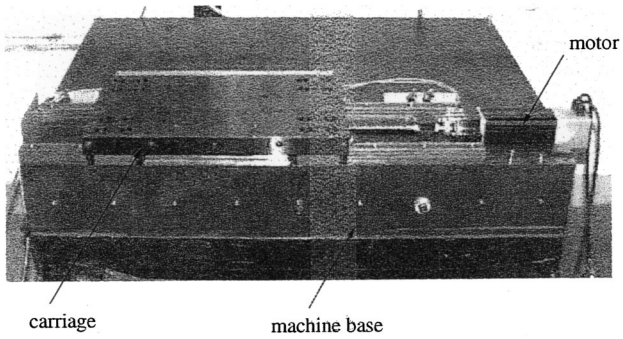

Fig. 3 Photograph of the small ball-screw stage showing the machine base, carriage, and motor

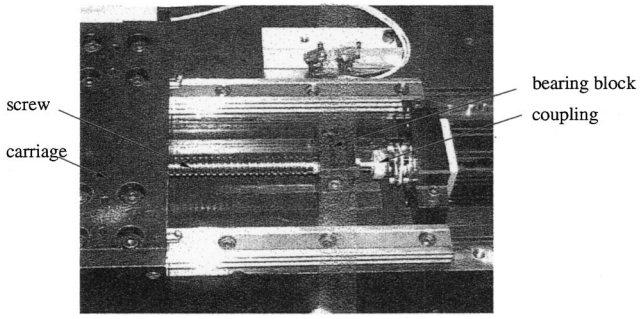

Fig. 4 Photograph of the small ball-screw stage showing the carriage, screw, bearing block, and coupling

Using this value along with the numbers given in Table 1, we predict the axial resonance to occur at 194 Hz and the non-minimum phase zero to occur at 975 Hz. It is difficult to predict the damping in such a system from first principles, but based on experience we expect the system to exhibit a loss factor of about 0.02 (equivalent to a viscous damping ratio ζ of 0.01). We therefore set both C_c and C_m to zero and simply associate this loss factor with the overall stiffness of the screw when generating the transfer function plotted in Fig. 6.

3.1.1 Transfer Functions. The transfer function from motor torque to carriage position is measured by exciting the motor with a sinusoidal torque and measuring the response from the linear encoder. A schematic of the experimental setup is shown in the

Table 1 Important parameters of ball-screw drive shown in Fig. 3

Ball-screw average diameter (d)	16.0 mm
Ball-screw lead (ℓ)	5.08 mm
Ball-screw length between bearing supports (L)	406.4 mm
Ball-screw material	steel
Ball-nut stiffness (K_n)	260 N/μm
Combined bearing and housing stiffness (k_{b1}) (measured)	51 N/μm
Torsional stiffness of coupling (κ_c)	693 N·m
Motor inertia (J_m)	7.8×10^{-5} kg·m^2
Carriage Mass (m_c)	25 kg

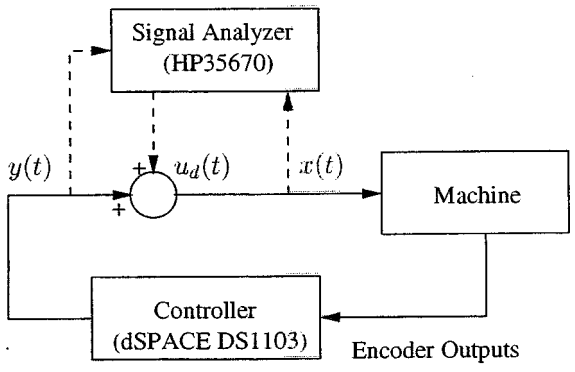

Fig. 5 Schematic of sine-sweep experiments. The signals $x(t)$, $y(t)$, and $u_d(t)$ are the power amplifier input, DAC output, and swept sine disturbance, respectively. The required transfer function is $Y(s)/X(s)$

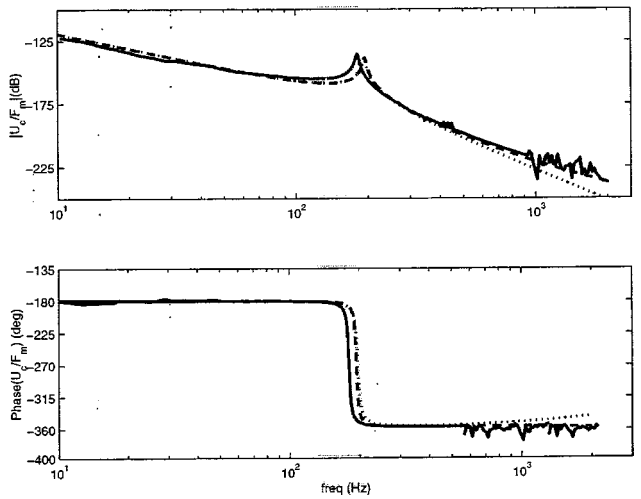

Fig. 6 Measured and predicted transfer function from motor torque to linear encoder for the stage of Fig. 3: measured (solid line), predicted (dashed line), and predicted if the non-minimum-phase zero is neglected (dotted line)

Fig. 5. The stage is set up under closed-loop control using a PC-based DSP board (dSPACE DS1103 [19]), and a disturbance signal is input to the system at a summing junction formed at the input terminal of the power amplifier of the motor. An HP35670A signal analyzer is used to generate a sinusoidal disturbance, measure the input and output signals, and determine their relative magnitude and phase.

The resulting transfer function agrees well with that predicted by the model, as shown in Fig. 6. The measured loss factor and the resonance frequency associated with the axial resonance are 0.02 and 180 Hz, respectively. The non-minimum phase zero causes the magnitude of the response to roll off slowly (at -40 rather than -60 db per decade) at high frequencies with a phase of -360 deg. Its effect is clearly evident when the measured and predicted transfer functions are compared to that which would be predicted by neglecting it, plotted as a dotted line in Fig. 6.

3.2 Large Stage. A second set of experiments were conducted on the test stand shown in Figs. 7 and 8. It includes a ball-screw with lead and diameter of 25.4 mm and length 1100 mm (Table 2). The base is a weldment with internal constrained layer dampers as detailed by Varanasi [20]. A carriage whose mass

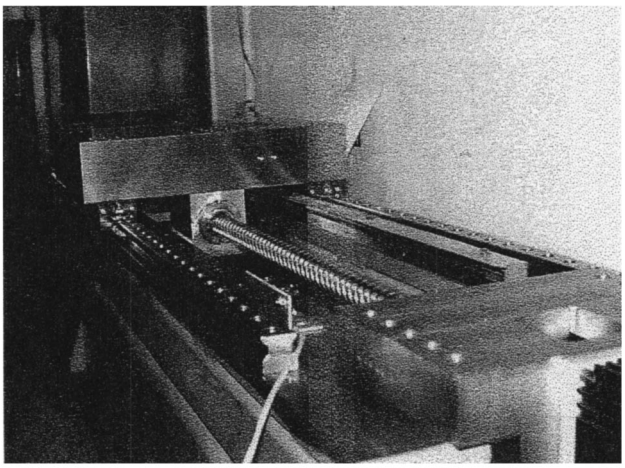

Fig. 7 Photograph of the large ball-screw stage

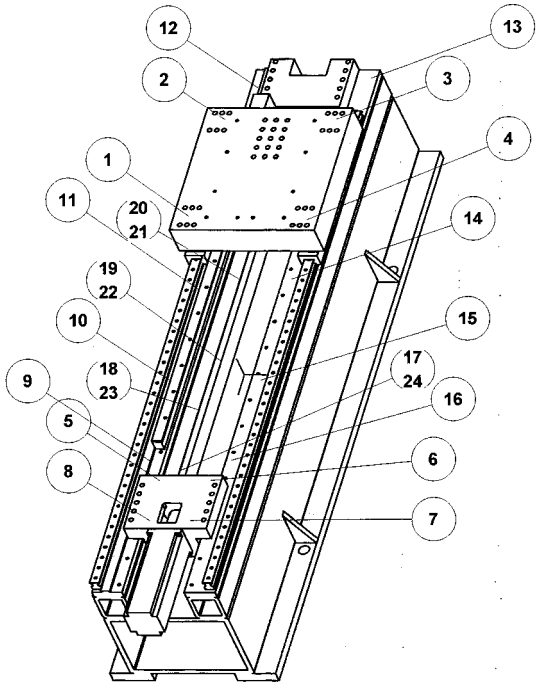

Fig. 8 Drawing of the large ball-screw stage showing measurement positions for modal experiment

is approximately 80 kg is mounted on Schneeberger MRD25 [21] roller guides and clamped to the ball-nut. The bearing support at the motor end consists of four 60-deg angular contact bearings mounted back to back. A brushless servomotor (Aerotech BM500 [17]) is attached to the screw by means of a bellows-type coupling (Gam KM12 [22]).

3.2.1 Transfer Functions. The system is set up initially with screw allowed to slide axially in the bearings farthest from the motor and the carriage near the end of its travel ($x_c = 813$ mm). Assuming a loss factor of 0.02 for the drive, we plot the predicted transfer functions from motor torque to motor rotation in Fig. 9 and from motor torque to carriage position in Fig. 10. These agree closely with the measured data, taken by using feedback from a motor encoder and a linear encoder, respectively.

Next, we install a viscoelastic damper at the thrust bearing farthest from the motor by inserting a thin washer of EAR-C1002 [23] damping material in series with four angular-contact bearings. The screw is preloaded in tension against these bearings, and because the damping washer is relatively complaint, thermal expansion of the screw leads to only a small decrease in the tensile preload of the screw. The expected complex stiffness of the viscoelastic washer (denoted k_v in Fig. 2) is $40(1 + j\ \mathrm{sgn}\ \omega)$ N/μm. Using this value, we expect to attain a loss factor of 0.18, and obtain from measurement a loss factor of 0.14. The predicted and measured transfer functions are shown in Figs. 11 and 12 and the

Table 2 Important parameters of ball-screw stage shown in Fig. 7

Ball-screw average diameter (d)	25.4 mm
Ball-screw lead (ℓ)	25.4 mm
Ball-screw length between bearing supports (L)	1100 mm
Ball-screw material	steel
Ball-nut stiffness (k_n)	3000 N/μm
Bearing stiffness (k_{b1})	6000 N/μm
Torsional stiffness of coupling (κ_c)	6800 N·m
Motor inertia (J_m)	13.9×10^{-5} kg·m^2
Carriage Mass (m_c)	80 kg

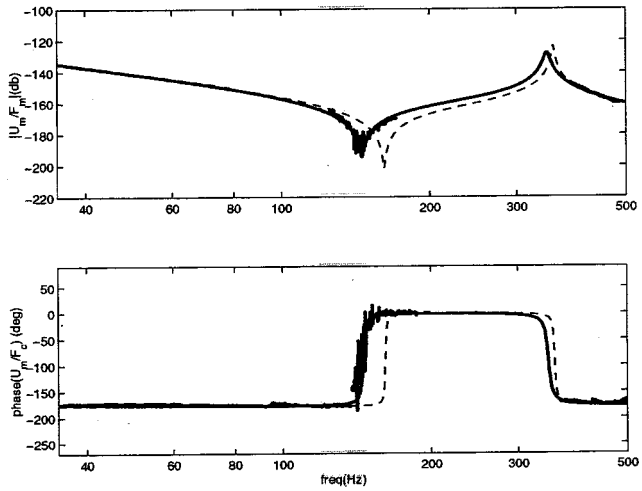

Fig. 9 Measured (solid line) and predicted (dashed line) collocated transfer functions of the large stage without viscoelastic damper

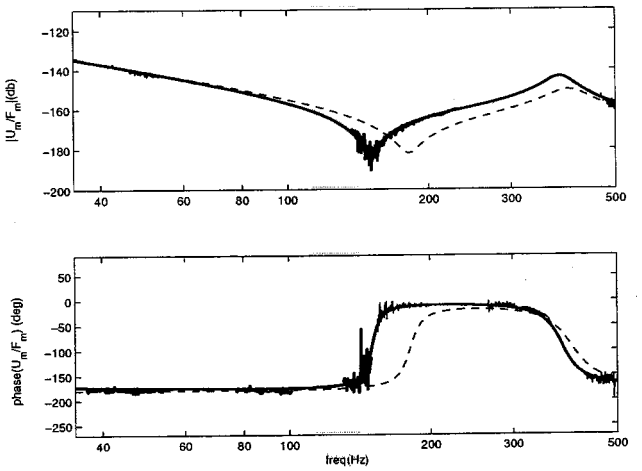

Fig. 11 Measured (solid line) and predicted (dashed line) collocated transfer function of the large stage with a viscoelastic damper installed

results are summarized in Table 3. According to the model, the non-minimum phase zero should appear at approximately 1500 Hz, but our measurements become obscured by quantization errors at frequencies above about 450 Hz as the magnitude of the response rolls off.

Comparison of the predicted and measured responses shows that the resonant frequencies are overestimated by as much as 4% in the worst case. This may be attributed to various compliances and inertias which are neglected in our calculations, such as those arising from flexure of the base or contact of the bearing blocks and the base.

3.2.2 Modal Tests. In Fig. 8, we show the location of the excitation and measurement positions employed in modal tests of the machine. An electromagnetic shaker is used to apply a random excitation close to point number 3 via a force transducer (PCB 208B [24]). The response is measured using a triaxial accelerometer (PCB 356B08 [24]) at each of the 24 points shown in Fig. 8. The points 1 through 4 are located on the four corners of the carriage, 5 through 8 on the motor-side bearing block, and 9 through 16 on the linear guide surfaces of the machine base. On the screw itself, the measurement points 17 through 24 are chosen to be diametrically opposite in order to capture the stretching and twisting motion of the screw. The force sensor and the accelerometer are connected to a signal analyzer (HP35670A) to obtain the force-to-acceleration transfer functions, from which the resonant frequencies, damping ratios, and mode shapes are extracted.

In Fig. 13, we show (in plan view) a series of snapshots of the first flexible mode of the system starting from the undeformed position. From the figure, we see that this mode corresponds to axial motion of the carriage accompanied by stretch and twist of the screw, in agreement with the model. The measured resonant frequency and damping ratio closely match those obtained from the sine-sweep experiments.

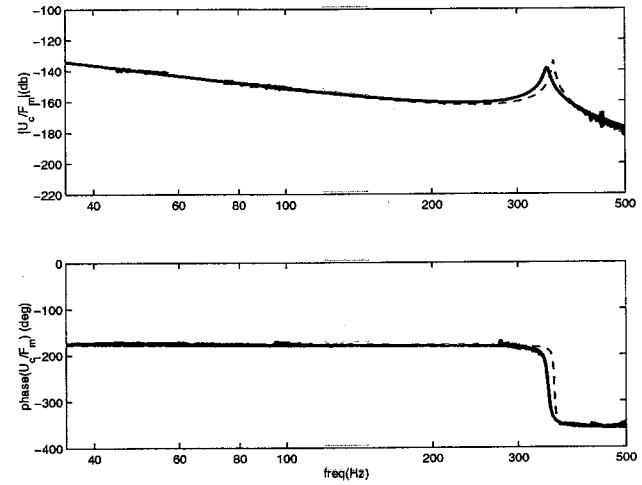

Fig. 10 Measured (solid line) and predicted (dashed line) noncollocated transfer functions of the large stage without viscoelastic damper

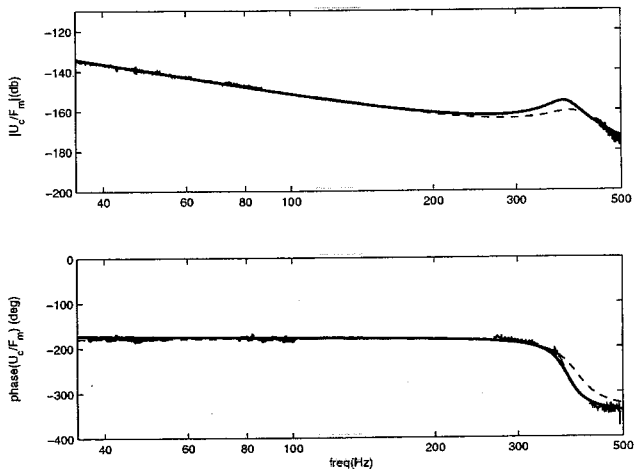

Fig. 12 Measured (solid line) and predicted (dashed line) noncollocated transfer function of the large stage with a viscoelastic damper installed

Table 3 Predicted and measured resonance frequencies and loss factors from sine-sweep experiments

	predicted		measured	
	freq (Hz)	η	freq (Hz)	η
free end	360	0.02	349	0.04
damped end	400	0.18	382	0.14

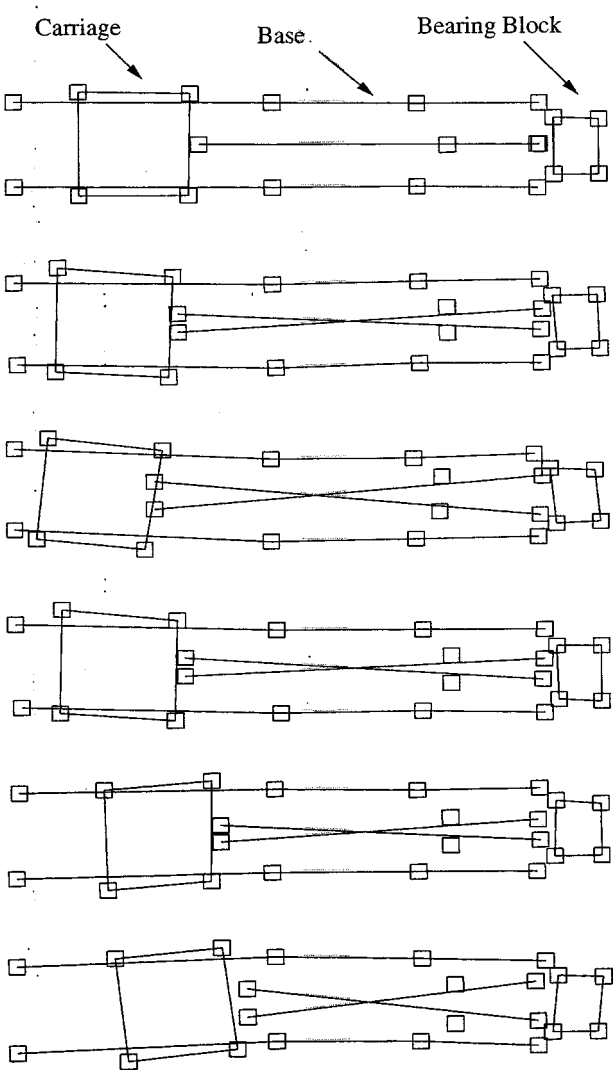

Fig. 13 Measured axial mode shape of the large ball-screw test stand at 349 Hz with loss factor of 0.04. The figure shows snapshots of the mode starting from undeformed position. The small squares indicate measurement locations.

4 Conclusion

The closed-loop performance of lead-screw drive systems is limited by a drive resonance in which kinetic energy is stored in the carriage, motor, and screw; potential energy is stored in the screw, bearings, and nut; and energy is dissipated primarily at material interfaces in the bearings, nut, or bolted joints. For most designs, this resonance is associated with a mode shape in which the torsional and extensional strains in the screw are uniform along the portions of the screw between thrust bearings and nut. We parameterize this shape by the displacements of the motor and carriage, and use it in a Galerkin procedure to derive a reduced-order model of the lead-screw system. Energy dissipation is accounted for in the model by both hysteretic and viscous damping.

For light damping, a perturbation expansion yields simple formulas for the open-loop poles of the system, from which we obtain an equivalent viscously damped model and the transfer functions from motor torque to motor rotation and carriage position. Experiments conducted on a pair of ball-screw stages confirm that the model accurately predicts the open-loop transfer functions, including the location of a non-minimum-phase zero in the transfer function from motor torque to carriage position.

The impact of the drive resonance on performance is strongly influenced by the damping in the system. The energy dissipated in traditional materials of construction (such as steel, cast iron, or aluminum) is usually negligible compared to that dissipated by microslip in bearings and joints. This damping is difficult to predict and often varies with the temperature and state of lubrication in a machine. A viscoelastic damper incorporated into one of the thrust bearings that support a lead-screw provides predictable and relatively high damping without the need for very high preload forces.

The model presented in this paper forms the basis for a design procedure for high-performance drives operated with feedback control [20,25]. Unless packaging constraints are severe, it is usually possible to choose the thrust bearings, ball nut, coupling, and their associated mounts to be much stiffer than the screw itself; this produces a relatively stiff drive and allows a considerable simplification in the terms that appear in the mass and stiffness matrices. Next, a viscoelastic damper is chosen to produce a known loss factor in the drive resonance. Along with the important mechanical design parameters such as the lead and diameter of the screw, a controller of a given form can be parameterized with reasonable constraints. Finally, the combined set of parameters can be optimized to maximize desired performance measures, such as the closed-loop bandwidth or settling time.

Acknowledgment

The authors wish to thank Profs. Alexander Slocum and David Trumper, both of MIT, for valuable advice on the construction of the stages used in the experiments and the characterization of their dynamics.

References

[1] Chen, Y., and Tlusty, J., 1995, ''Effect of Low-Friction Guideways and Lead-Screw Flexibility on Dynamics of High-Speed Machines,'' Annals of the CIRP, **44**, pp. 353–356.
[2] Tlusty, J., 2000, *Manufacturing Processes and Equipment*, Prentice Hall, Upper Saddle River, New Jersey.
[3] Smith, D. A., 1999, ''Wide Bandwidth Control of High-Speed Milling Machine Feed Drives,'' Ph.D. thesis, University of Florida, Gainesville, Florida.
[4] Smith, M. H., Annaswamy, A. M., and Slocum, A. H., 1995, ''Adaptive Control Strategies for a Precision Machine Tool Axis,'' Precision Engineering, **17**(3), pp. 192–206.
[5] Lim, H., Seo, J-W., Choi, C-H., 2000, ''Position Control of XY Table in CNC Machining Center with Non-rigid Ballscrew,'' *Proceedings of the American Control Conference*, pp. 1542–1546, Chicago, Illinois.
[6] Nayfeh, S. A., 1998, ''Design and Application of Damped Machine Elements,'' Ph.D. thesis, Massachusetts Institute of Technology, Cambridge, Massachusetts.
[7] Nayfeh, S. A., and Slocum, A. H., 1998, ''Enhancing Ball-screw Axial Dynamics,'' *Proceedings of the ASPE 13th Annual Meeting*, St. Louis, Missouri.
[8] Book, W. J., 1993, ''Controlled Motion in an Elastic World,'' ASME J. Dyn. Syst., Meas., Control, **115**, pp. 252–261.
[9] Meirovitch, L., 1980, *Computational Methods in Structural Dynamics*, Sijthoff & Noordhoff, Rockville, Maryland.
[10] Lowenfeld, K., 1959, ''Zusatzdämpfung von Werkzeugmaschinen durch Lamellenpakete,'' Maschinenmarkt No. 19.
[11] Koenigsberger, F., and Tlusty, J., 1970, *Machine Tool Structures*, Pergammon Press, London.
[12] Nashif, A. D., Jones, D. I. G., and Henderson, J. P., 1985, *Vibration Damping*, John Wiley, New York.
[13] Crandall, S. H., 1991, ''The Hysteretic Damping Model in Vibration Theory,'' Rep. Sci. Res. Inst., **25**, pp. 23–28.
[14] Freudenberg, J. S., and Looze, D. P., 1985, ''Right Half Plane Poles and Zeros and Design Tradeoffs in Feedback Systems,'' IEEE Trans. Autom. Control, **30**(6), pp. 555–565.
[15] Spector, V. A., and Flashner, H., 1990, ''Modeling and Design Implications of Noncollocated Control in Flexible Systems,'' ASME J. Dyn. Syst., Meas., Control, **112**, pp. 186–193.
[16] Hochmuth, C. A., 1990, ''Design and Construction of a Machine Tool Axis Prototype for Evaluation of Adaptive and Learning Control Systems,'' S. M. thesis, Massachusetts Institute of Technology, Cambridge, Massachusetts.

[17] Aerotech Inc., Pittsburgh, Pennsylvania.
[18] Renbrandt Flexible Couplings Inc., Boston, Massachusetts.
[19] dSPACE Inc., Novi, Michigan.
[20] Varanasi, K. K., 2002, ''On the Design of a Precision Machine for Closed-Loop Performance,'' S. M. thesis, Massachusetts Institute of Technology, Cambridge, Massachusetts.
[21] Schneeberger Inc., Bedford, Massachusetts.
[22] Gam Servo Couplings, Harwood Heights, Illinois.
[23] E-A-R Speciality Composites, Indianapolis, Indiana.
[24] PCB Piezotronics, Depew, New York.
[25] Varanasi, K. K., and Nayfeh, S. A., 2001, ''Modeling, Identification, and Control of Ballscrew Drives,'' *Proceedings of the ASPE 16th Annual Meeting*, Crystal City, Virginia.